Two-parameter Persistence for Images via Distance Transform

Chuan-Shen Hu
Dept. of Maths
NTNU, Taiwan
peterbill26@hotmail.com

Austin Lawson
Program
UNCG, USA
alawso50@utk.edu

Yu-Min Chung*
Eli Lilly and Company
Indianapolis, USA
yumchung@alumni.iu.edu

Kaitlin Keegan†
Program
UNR, USA
kkeegan@unr.edu

Abstract

The distance transform of a binary image is a classic tool in computer vision and it has been widely used in the field of Topological Data Analysis (TDA) to study porous media. A common practice is to convert grayscale images to binary ones to apply the distance transform. In this work, by considering the threshold decomposition of a grayscale image, we prove that threshold decomposition and distance transform together to formulate a two-parameter filtration. This would offer the TDA community a concrete example to apply multi-parameter persistence on digital image analysis. We demonstrate our method on the firn dataset.

1. Introduction

Topological data analysis (TDA) is a rising field at the intersection of Mathematics, Statistics, and Machine Learning [9, 3, 33, 5]. Tools from TDA have proven successful in analyzing a variety of scientific problems and datasets (see e.g. [25] for a list of application areas). The development of the *persistent homology* is the main driving force in TDA (see e.g. introductory texts [6, 35]). In classical persistent homology, we track changes in homology over a one-parameter *filtration*, or a single sequence of spaces satisfying a nested subset relation ordered by inclusion. Recently, a more general form of persistent homology, multiparameter persistent homology has been studied [11, 19, 4, 27, 20]. Similar to the classic filtration, multiparameter persistence uses a *multi-parameter filtration*. However, to the best of our knowledge, multi-parameter filtration in the computer vision literature is limited. In this paper, we provide a concrete two-parameter filtration for 2D or 3D digital images.

Our motivation for this study is the analysis of firn data. *Firn* is a type of porous media that is formed at the top of glaciers and ice sheets where snow melting rarely occurs. This area of firn, or old snow layers, comprises metamorphosing ice particles and interconnected pore space. Understanding how the underlying microstructure of the firn changes with depth is a difficult, yet important, task that is required for better interpretation of satellite remote sensing signals and ice core paleoclimate records. A non-destructive method for retrieving firn microstructural information is x-ray micro-computed tomography (micro-CT). Micro-CT imaging of firn sample produces a stack of 2-dimensional cross-sectional images in greyscale, that represent the 3-dimensional volume of the sample.

There have been several studies that analyze porous media with tools in TDA. For instance, in [21], authors develop statistical inference of persistent homology over 3D rock images to predict fluid flow; in [15], authors develop a new index based on persistent homology to characterize the degree of rock heterogeneity; in [13], authors use persistent homology to relate microstructure and fluid trapping in sandstones; in [30], authors study pore space and fluid phase characterization in sands; in [26], authors study percolating length scales; in [17], authors study evolution of a cell aluminium foam. The common pipeline of these work is to (1) convert grayscale images to binary ones, (2) apply distance transform (defined in Section 2.2) to those binary images, and (3) use persistent homology to study transformed images.

In this paper, we extend the above pipeline by expanding (1); we consider all possible binary images obtained from threshold decomposition. For each resulting binary image, we proceed down the pipeline. Most importantly, we prove that the thresholding decomposition and distance transform formulate a two-parameter filtration. Thus, our main contribution to the field results in a new tool for practitioners to use in applications and many concrete examples for those researching multiparameter persistence to use while testing and exploring theories.

*This work was done when Chung was employed at the Department of Mathematics and Statistics, University of North Carolina at Greensboro.

†Keegan were partially supported by the Army Research Office under Grant Number W911NF-20-1-0131. The views and conclusions contained in this document are those of the authors and should not be interpreted as representing the official policies, either expressed or implied, of the Army Research Office or the U.S. Government. The U.S. Government is authorized to reproduce and distribute reprints for Government purposes notwithstanding any copyright notation herein.

Our paper is outlined as follows. We introduce necessary mathematical backgrounds for this work, including notations, distance transform, persistent homology, and two-parameter filtration in Section 2. In Section 3, we prove our main result – the combination of distance transform and thresholding operation forms a two-parameter filtration. Finally, in Section 4, we extract useful information from the two-parameter filtration and apply it to the firn data.

2. Background and Notation

This section is split into three parts. First, we review notations and basic properties of digital images used in this paper. Next, we introduce the distance transform of digital images and its connection to the filtration of images. We follow notations in the work [29, 28, 22]. Finally, we give a brief introduction to persistent homology.

2.1. Digital Images

We use $\mathbb{R}$ to denote the set of all real numbers. The set of all *non-negative real numbers* is denoted by $\mathbb{R}_{\geq 0} = \{a \in \mathbb{R} : a \geq 0\}$. Similarly, $\mathbb{Z}_{\geq 0}$ is the set of all non-negative integers.

An *image domain* in $\mathbb{Z}^2$ means a non-empty and finite subset of $\mathbb{Z}^2$. Let P be an image domain in $\mathbb{Z}^2$. An (*digital*) *image* is referred as a function $f : P \to \mathbb{R}_{\geq 0}$. The set of all images on P is denoted by $\mathcal{I}_P$. An image $f \in \mathcal{I}_P$ is called *binary* if it has range $\{0, 1\}$. Typically, 0 and 1 represent black and white color, respectively. The set of all binary images on $P \subseteq \mathbb{Z}^2$ is denoted by $\mathcal{BI}_P$. An image $f \in \mathcal{I}_P$ which is not binary is called a *grayscale image*. Based on this setting, we have $\mathcal{BI}_P \subseteq \mathcal{I}_P$. One can also define an order in $\mathcal{I}_P$. For two functions $f, g : P \to \mathbb{R}$, we say that $f \leq g$ if and only if $f(\mathbf{p}) \leq g(\mathbf{p})$ whenever $\mathbf{p} \in P$.

For illustration, we also use the following convention to represent an image f on the grid P:

$$P = \begin{matrix} \bullet & \bullet \\ \bullet & \bullet \end{matrix} \text{ and } f = \begin{matrix} a & b \\ c & d \end{matrix} \tag{1}$$

where $a, b, c, d \in \mathbb{R}_{\geq 0}$. In this case, P is a 2-by-2 grid. and the corresponding pixel values are a, b, c, b, respectively.

Let $f \in \mathcal{I}_P$. The *support* of f is defined by

$$\operatorname{supp}(f) = \{\mathbf{p} \in P \mid f(\mathbf{p}) \neq 0\}. \tag{2}$$

In particular, the support of a binary image is the set of all white pixels.

Given a grayscale image $f \in \mathcal{I}_P$, the binary image thresholded at t is defined as

$$f_t(\mathbf{p}) := \begin{cases} 0 & \text{if } f(\mathbf{p}) \leq t, \\ 1 & \text{otherwise} \end{cases} \tag{3}$$

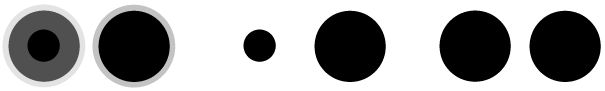

(a) Image f (b) Image f_{79} (c) Image f_{194}

Figure 1. An example of the thresholding operator. (a) A greyscale image f which has size 800×600 pixels. The range of the pixel values of f is $\{0, 80, 195, 227, 255\}$. Figures (b) and (c) are images created by applying thresholds 79 and 194 on the image f.

for every $\mathbf{p} \in P \subseteq \mathbb{Z}^2$. Let f be an 8-bit grayscale image, the threshold decomposition of f is the collection of all possible binary images, $f_0,\ f_1,\ \cdots, f_{255}$. One may verify the following relation

$$f_t \leq f_s, \quad \text{if } s \leq t. \tag{4}$$

The following properties are used in the paper.

Proposition 1 ([29], Property 1.11)**.** *Let $f, g \in \mathcal{I}_P$ be images. If $f \leq g$, then $g^{-1}(0) \subseteq f^{-1}(0)$. In addition, if $f, g \in \mathcal{BI}_P$ are binary images, then $f \leq g$ if and only if $g^{-1}(0) \subseteq f^{-1}(0)$.*

The following proposition is an alternate form of Proposition 1.

Proposition 2. *For $f, g \in \mathcal{I}_P$. If $f \leq g$, then $\operatorname{supp}(f) \subseteq \operatorname{supp}(g)$. In addition, if $f, g \in \mathcal{BI}_P$ are binary images, then $\operatorname{supp}(f) \subseteq \operatorname{supp}(g)$ if and only if $f \leq g$.*

Proposition 3 ([14], Lemma 1)**.** *For images $f, g \in \mathcal{I}_P$, $f \leq g$ if and only if $f_t \leq g_t$ for every $t \in \mathbb{R}_{\geq 0}$.*

For example, the image f in Figure 1 contains two balls with different pixel values, where parts near the center of a ball have darker colors (i.e., lower pixel values). As a topographic map, different thresholds capture objects in different depths. In Figure 1-(b), the threshold 79 detects the darkest parts of two balls. On the other hand, the threshold 194 identifies all gray regions of the left ball as a single one and erodes the pixels of the value 227 in the right ball.

Figure 1 shows that different thresholds detect different objects. In this case, the sizes of the two balls lead to different distances between them. The distance transform in image processing provides a way to describe this relationship between local objects in digital images. In this work, we would combine the thresholding and distance transform techniques to study the firn data.

2.2. Distance Transform

In this subsection, we will review the notations for the distance transform which we follow [29, 28, 22] and discuss its properties.

Let $P \subseteq \mathbb{Z}^2$ be an image domain. Let d be a metric on P. The common choices of d are ∞-norm defined by

$$d_\infty((x_1, y_1), (x_2, y_2)) = \max\{|x_1 - x_2|, |y_1 - y_2|\}, \quad (5)$$

or q-norm defined by

$$d_q((x_1, y_1), (x_1, y_2)) := (|x_1 - x_2|^q + |y_1 - y_2|^q)^{1/q}. \quad (6)$$

In particular, d_∞ is also known as Chebyshev distance [2], d_1 is known as the taxicab metric [18], and d_2 is known as the Euclidean distance.

The definition of the distance transform is as following.

Definition. *Let $P \subseteq \mathbb{Z}^2$ be an image domain, $f \in \mathcal{I}_P$, and d be a metric on P. A **distance transform** with respect to metric d is a function $T_d : \mathcal{I}_P \to \mathcal{I}_P$ which is defined by*

$$T_d(f)(\mathbf{x}) = \min\{d(\mathbf{x}, \mathbf{y}) : \mathbf{y} \in \mathrm{supp}(f)\}, \ \forall\, \mathbf{x} \in P. \quad (7)$$

By switching the support of an image, the *anti-distance transform* can be defined.

Definition. *Let $P \subseteq \mathbb{Z}^2$ be an image domain, and $d : P \times P \to \mathbb{R}_{\geq 0}$ be a distance function. An **anti-distance transform** with respect to metric d is a function $\widetilde{T}_d : \mathcal{I}_P \to \mathcal{I}_P$ defined by*

$$\begin{aligned}\widetilde{T}_d(f)(\mathbf{x}) &= \min\{d(\mathbf{x}, \mathbf{y}) : \mathbf{y} \in P \setminus \mathrm{supp}(f)\} \\ &= \min\{d(\mathbf{x}, \mathbf{y}) : \mathbf{y} \in P, f(\mathbf{y}) = 0\}, \ \forall\, \mathbf{x} \in P.\end{aligned} \quad (8)$$

Remark. *We note that $T_d(f)$ (resp. $\widetilde{T}_d(f)$) is not defined here if $\mathrm{supp}(f) = \emptyset$ (resp. $P \setminus \mathrm{supp}(f) = \emptyset$). We omit these cases of images. However, one may consider the extended real number system to solve this logic issue [24].*

Distance and anti-distance transforms are tools for investigating the distribution of pixels. In this paper, we mainly consider distance and anti-distance transforms applying on binary images. In this case, as functions, these transforms would send each binary image to a grayscale one, i.e.

$$f \in \mathcal{BI}_P \implies T_d(f) \in \mathcal{I}_P. \quad (9)$$

Example 1. *Consider image $f : P \to \{0, 1\}$ with $P \subseteq \mathbb{Z}^2$ defined by*

$$f = \begin{matrix}1 & 1 & 1\\ 1 & 0 & 0\\ 1 & 0 & 0\end{matrix} \text{ with } P = \begin{matrix}\bullet & \bullet & \bullet\\ \bullet & \bullet & \bullet\\ \bullet & \bullet & \bullet\end{matrix} \quad (10)$$

and d_2. Then

$$T_{d_2}(f) = \begin{matrix}0 & 0 & 0\\ 0 & 1 & 1\\ 0 & 1 & 2\end{matrix} \text{ and } \widetilde{T}_{d_2}(f) = \begin{matrix}\sqrt{2} & 1 & 1\\ 1 & 0 & 0\\ 1 & 0 & 0\end{matrix}. \quad (11)$$

As shown in Example 1, each entry in $T_{d_2}(f)$ (resp. $\widetilde{T}_{d_2}(f)$) is the minimal distance of current pixel to a white (resp. black) component in image f. Combining two distance transforms $T_d(f)$ and $\widetilde{T}_d(f)$ leads to the *Signed Euclidean Distance Transform (SEDT)* [34]. Specifically, let $f \in \mathcal{BI}_P$, the SEDT is $\mathcal{T}_d(f) := T_d(f) - \widetilde{T}_d(f)$. Since we consider $T_d(f)$ and $\widetilde{T}_d(f)$ separately, our main result will also hold for SEDT.

Filtration of objects (or sets) is crucial for constructing persistent homology in TDA [23, 8]. We call a sequence of images $f_1, f_2, ..., f_n \in \mathcal{I}_P$ a *filtration* of images if

$$f_1 \leq f_2 \leq \cdots \leq f_n. \quad (12)$$

There several methods for obtaining a filtration of sets from a sequence of images. For instance, one may consider the preimages of zeros of images in (12):

$$f_n^{-1}(0) \subseteq \cdots \subseteq f_2^{-1}(0) \subseteq f_1^{-1}(0). \quad (13)$$

On the other hand, one can construct a filtration of sets by considering their supports:

$$\mathrm{supp}(f_1) \subseteq \mathrm{supp}(f_2) \subseteq \cdots \subseteq \mathrm{supp}(f_n). \quad (14)$$

The following proposition is useful for constructing filtration of images from distance transform.

Proposition 4. *Let $P \subseteq \mathbb{Z}^2$ be an image domain, d a metric on P, and $f, g \in \mathcal{I}_P$. Then the following hold:*

(a) $T_d(g) \leq T_d(f)$ *if* $\mathrm{supp}(f) \subseteq \mathrm{supp}(g)$*;*

(b) $\widetilde{T}_d(f) \leq \widetilde{T}_d(g)$ *if* $\mathrm{supp}(f) \subseteq \mathrm{supp}(g)$.

Hence $\mathcal{T}_d(g) \leq \mathcal{T}_d(f)$ if and only if $\mathrm{supp}(f) \subseteq \mathrm{supp}(g)$.

Proof. (a) If $\mathbf{x} \in P$, then $T_d(g)(\mathbf{x}) = \min\{d(\mathbf{x}, \mathbf{y}) : \mathbf{y} \in \mathrm{supp}(g)\}$. Because $\mathrm{supp}(f) \subseteq \mathrm{supp}(g)$, $T_d(g)(\mathbf{x}) = \min\{d(\mathbf{x}, \mathbf{y}) : \mathbf{y} \in \mathrm{supp}(g)\} \leq \min\{d(\mathbf{x}, \mathbf{y}) : \mathbf{y} \in \mathrm{supp}(f)\} = T_d(f)(\mathbf{x})$. Because $P \setminus \mathrm{supp}(g) \subseteq P \setminus \mathrm{supp}(f)$, (b) follows by the same arguments as in (a).

Conversely, if $\mathrm{supp}(f) \nsubseteq \mathrm{supp}(g)$, then there is an $\mathbf{x} \in P$ such that $f(\mathbf{x}) > 0$ and $g(\mathbf{x}) = 0$. This shows that $T_d(f)(\mathbf{x}) = 0$ and $T_d(g)(\mathbf{x}) > 0$. Hence $T_d(g) \nleq T_d(f)$. □

Remark. *We note that the filtrations in* (13) *and* (14) *only work for the case of $f_1, ..., f_n \in \mathcal{I}_P$. Because $\mathcal{T}_d(f_i)$ may contains negative entries,* (13) *and* (14) *may not hold. However, by Proposition 4, we may obtain a filtration of sets* $\mathrm{supp}(f_n) \subseteq \cdots \subseteq \mathrm{supp}(f_2) \subseteq \mathrm{supp}(f_1)$ *if $T_d(f_1) \leq T_d(f_2) \leq \cdots \leq T_d(f_n)$.*

Figure 2 illustrates how the distance transform captures the distance information in digital images. In this figure, images in (c) and (d) are the heat maps of binary images in

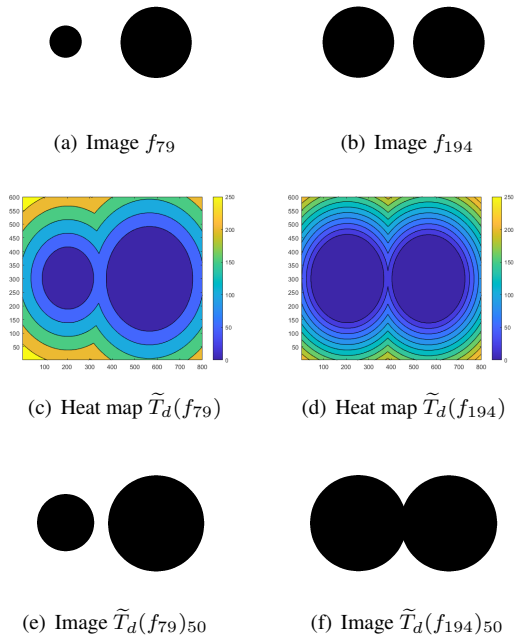

(a) Image f_{79} (b) Image f_{194}

(c) Heat map $\widetilde{T}_d(f_{79})$ (d) Heat map $\widetilde{T}_d(f_{194})$

(e) Image $\widetilde{T}_d(f_{79})_{50}$ (f) Image $\widetilde{T}_d(f_{194})_{50}$

Figure 2. An example of the distance transforms on images. (a) and (b) are the images f_{79} and f_{194} defined in Figure 1. (c) and (d) are the heat maps $\widetilde{T}_d(f_{79})$ and $\widetilde{T}_d(f_{194})$ of the images f_{79} and f_{194}. Images in (e) and (f) are obtained by applying the threshold 50 on the heat maps in (c) and (d). The distance d used here is the Euclidean distance.

(a) and (b). By viewing each heat map as a greyscale image, the value of a pixel in a heat map made by the anti-distance transform is the minimal distance from the pixel to the black regions in the original binary image.

For example, in Figure 2, colors in $\widetilde{T}_d(f_{79})$ represent the values of minimal distances between pixels to black regions in f_{79}. For the fixed threshold 50, $\widetilde{T}_d(f_{79})_{50}$ is a binary image where pixels in $\widetilde{T}_d(f_{79})_{50}$ are black if they have distance values ≤ 50.

The set of black pixels in f_{79} is contained in the set of black pixels in $\widetilde{T}_d(f_{79})_{50}$. In this case, the information of connected components in f_{79} and $\widetilde{T}_d(f_{79})_{50}$ are the same. On the other hand, $\widetilde{T}_d(f_{194})_{50}$ changes the number of connected components in f_{194} since the balls in f_{194} are finally merged into a single component.

Homology, a mathematical tool developed in algebraic topology [10, 12, 32], can measure this topological information. As the thresholds change, one greyscale image f may uncover various topologies. It motivates us to integrate the persistent homology into this framework. The framework of changing the 2-parametric thresholds derives a double sequence of images. In this paper, we call this double sequence a bi-filtration of images and prove that it satisfies the set inclusion relation (Proposition 5).

2.3. Persistent Homology

Homology is a tool from Algebraic Topology that allows topologists to assign abstract topological spaces to computable vector spaces [10, 12, 32]. We will not define it here, but for our purposes, homology helps us count the number of holes in a topological space. For example, if X is a topological space, $H_0(X)$ helps us count the number of 0-dimensional holes, or connected components, of X. To be more precise, $H_0(X)$ produces a vector space whose dimension, denoted β_0 is called the zeroth *Betti number*. In a similar way, $H_1(X)$ produces β_1, a count of the one-dimensional holes in X, and $H_2(X)$ produces β_2, which counts the number of "air pockets" in X. The index and heuristic continue for H_n, $n \in \mathbb{N}$. In TDA, we typically concern ourselves only with H_0, H_1, and H_2.

On the other hand, *persistent homology* [7, 3] lets us compute and track homology over related spaces. A *filtration of topological spaces* is an increasing sequence of topological spaces

$$X_1 \subseteq X_2 \subseteq \cdots \subseteq X_m. \tag{15}$$

For a given non-negative integer $n \in \mathbb{Z}_{\geq 0}$, we can compute $H_n(X_i)$ for $i = 1, \ldots m$. Due to the subset relations, we are guaranteed linear maps $f_{ij} : X_i \to X_j, i \leq j$ between the resulting spaces.

We say a homology class α is *born* at b if we have $\alpha \in H_k(X_b)$ and $\alpha \notin \operatorname{im} f_{b-1,b}$. We say that α born at b **dies** at d, $d \geq b$ if $f_{b,d-1}(\alpha) \notin \operatorname{im} f_{b-1,d-1}$, but $f_{b,d}(\alpha) \in \operatorname{im} f_{b-1,d}$, i.e. if it merges with a previous class. In the case where a class does not die, we assign it a death value of ∞.

We collect the birth-death pairs (b, d) for each class appearing in the filtration into a summary called a *persistence diagram*, or just *diagram* associated to the filtration, $\{X_i\}_{i=1}^m$, which we will denote by $D(\{X_i\}_{i=1}^m)$.

To apply persistent homology to images, we note that we can assign topological spaces, called cubical sets to binary images. Moreover, we can use a homology theory called cubical homology to compute homology on such spaces [16]. Thus for a given grayscale image, our filtration is exactly the threshold decomposition across all threshold values. From here, the persistent homology discussion above applies.

We use images in Figure 3 to explain the geometric meaning of the persistence diagrams of a filtration. For the image f in Figure 1, the collections of black pixels in images $\widetilde{T}_d(f_{79})_j$, $j = 1, 2, ..., 255$ form a filtration of cubes. The barcode $(1, 78)$ in the 0^{th} persistence diagram of this filtration is an approximation for the (half of) distance between the balls in f_{79}.

In this paper, we focus on filtrations induced by f_i for $i = 1, 2, ..., 255$. We will prove in the next section that filtrations associated with different binary images f_i's also

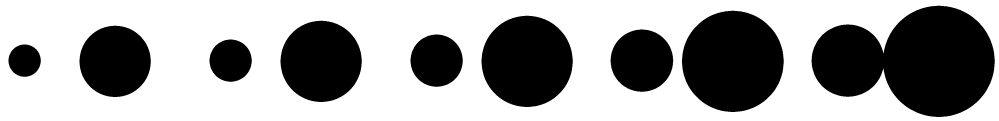

(a) f_{79} (b) $\widetilde{T}_d(f_{79})_{20}$ (c) $\widetilde{T}_d(f_{79})_{40}$ (d) $\widetilde{T}_d(f_{79})_{60}$ (e) $\widetilde{T}_d(f_{79})_{80}$

Figure 3. An example of a filtration made by applying different thresholds on a transformed image $\widetilde{T}_d(f_{79})$ where f is defined as in Figure 1. The 0^{th} persistence diagram of this filtration is $\{(1,+\infty),(1,78)\}$.

satisfy the set-inclusion relations, and hence form a bi-filtration of cubes.

3. Two-parameter Persistence via Distance Transform

In this section, we introduce how to construct a bi-filtration by applying distance transforms and thresholding on a digital image.

Before defining bi-filtration of sets, we first define an partial ordered $\leq$ on $\mathbb{Z}^2$. Given two vectors $\mathbf{u}=(x_1,y_1)$ and $\mathbf{v}=(x_2,y_2)$, we define $\mathbf{u}\leq\mathbf{v}$ if and only if $x_1\leq x_2$ and $y_1\leq y_2$.

Definition ([4]). *Let $\mathcal{N}$ be a subset of $\mathbb{Z}^2$, a **bi-filtration** of sets is a collection $\{S_{\mathbf{u}}\}_{\mathbf{u}\in\mathcal{N}}$ of sets indexed by $\mathcal{N}$ which satisfies $S_{\mathbf{u}}\subseteq S_{\mathbf{v}}$ whenever $\mathbf{u}\leq\mathbf{v}$.*

Let $P\subseteq\mathbb{Z}^2$ be an image domain and $f\in\mathcal{I}_P$. For $s\leq t\in\mathbb{R}_{\geq 0}$, we have $f_t\leq f_s$ where f_t and f_s are binary images. By Proposition 2, $\mathrm{supp}(f_t)\subseteq\mathrm{supp}(f_s)$. Therefore, for a distance function $d: P\times P\to\mathbb{R}_{\geq 0}$, if $t_1\geq t_2\geq\cdots\geq t_l\geq 0$, we can consider images $\widetilde{T}_d(f_{t_1})\leq\widetilde{T}_d(f_{t_2})\leq\cdots\leq\widetilde{T}_d(f_{t_l})$. On the other hand, if $a_1\geq a_2\geq\cdots\geq a_k\geq 0$, then $\widetilde{T}_d(f_{t_i})_{a_1}\leq\widetilde{T}_d(f_{t_i})_{a_2}\leq\cdots\leq\widetilde{T}_d(f_{t_i})_{a_k}$ for each $i\in\{1,2,...,l\}$ by Proposition 3. Finally, we obtain the net

$$\begin{array}{ccccc}
\widetilde{T}_d(f_{t_1})_{a_1} & \leq & \widetilde{T}_d(f_{t_1})_{a_2} & \leq\cdots\leq & \widetilde{T}_d(f_{t_1})_{a_k}\\
\wedge| & & \wedge| & \vdots & \wedge|\\
\widetilde{T}_d(f_{t_2})_{a_1} & \leq & \widetilde{T}_d(f_{t_2})_{a_2} & \leq\cdots\leq & \widetilde{T}_d(f_{t_2})_{a_k}\\
\wedge| & & \wedge| & \vdots & \wedge|\\
\widetilde{T}_d(f_{t_3})_{a_1} & \leq & \widetilde{T}_d(f_{t_3})_{a_2} & \leq\cdots\leq & \widetilde{T}_d(f_{t_3})_{a_k}\\
\wedge| & & \wedge| & \vdots & \wedge|\\
\vdots & & \vdots & \vdots & \vdots\\
\wedge| & & \wedge| & \vdots & \wedge|\\
\widetilde{T}_d(f_{t_l})_{a_1} & \leq & \widetilde{T}_d(f_{t_l})_{a_2} & \leq\cdots\leq & \widetilde{T}_d(f_{t_l})_{a_k}
\end{array} \tag{16}$$

of binary images. Alternatively, if we define

$$\widetilde{U}_{(t_i,a_j)}=\left(\widetilde{T}_d(f_{t_i})_{a_j}\right)^{-1}(0) \tag{17}$$

we have the bi-filtration

$$\begin{array}{ccccc}
\widetilde{U}_{(t_1,a_1)} & \supseteq & \widetilde{U}_{(t_1,a_2)} & \supseteq\cdots\supseteq & \widetilde{U}_{(t_1,a_k)}\\
\cup| & & \cup| & \vdots & \cup|\\
\widetilde{U}_{(t_2,a_1)} & \supseteq & \widetilde{U}_{(t_2,a_2)} & \supseteq\cdots\supseteq & \widetilde{U}_{(t_2,a_k)}\\
\cup| & & \cup| & \vdots & \cup|\\
\widetilde{U}_{(t_3,a_1)} & \supseteq & \widetilde{U}_{(t_3,a_2)} & \supseteq\cdots\supseteq & \widetilde{U}_{(t_3,a_k)}\\
\cup| & & \cup| & \vdots & \cup|\\
\vdots & & \vdots & \vdots & \vdots\\
\cup| & & \cup| & \vdots & \cup|\\
\widetilde{U}_{(t_l,a_1)} & \supseteq & \widetilde{U}_{(t_l,a_2)} & \supseteq\cdots\supseteq & \widetilde{U}_{(t_l,a_k)}
\end{array} \tag{18}$$

of black pixels in binary images. This defines a bi-filtration over the index set

$$\mathcal{N}=\{(t_i,a_j): i=1,...,l, j=1,2,...,k\}. \tag{19}$$

where $(t,a)\leq(s,b)$ in $\mathcal{N}$ is defined by $t\leq s$ and $a\leq b$.

We summarize the main result as the following proposition by computing filtrations for $\widetilde{T}_d$ and $\mathcal{T}_d$:

Proposition 5. *Let $P\subseteq\mathbb{Z}^2$ be an image domain, d a distance function on P, and $f\in\mathcal{I}_P$. For $s\leq t$ and $a\leq b$ in $\mathbb{R}_{\geq 0}$, the following order relations hold:*

$$\begin{array}{ccc}
T_d(f_t)_b & \leq & T_d(f_t)_a\\
\vee| & & \vee|\\
T_d(f_s)_b & \leq & T_d(f_s)_a
\end{array}, \tag{20}$$

$$\begin{array}{ccc}
\widetilde{T}_d(f_t)_b & \leq & \widetilde{T}_d(f_t)_a\\
\wedge| & & \wedge|\\
\widetilde{T}_d(f_s)_b & \leq & \widetilde{T}_d(f_s)_a
\end{array}, \tag{21}$$

and

$$\begin{array}{ccc}
\mathcal{T}_d(f_t)_b & \leq & \mathcal{T}_d(f_t)_a\\
\vee| & & \vee|\\
\mathcal{T}_d(f_s)_b & \leq & \mathcal{T}_d(f_s)_a
\end{array}. \tag{22}$$

In particular, if $\widetilde{U}_{(\alpha,\beta)}:=\left(\widetilde{T}_d(f_\alpha)_\beta\right)^{-1}(0)$, then (21) defines a bi-filtration of sets:

$$\begin{array}{ccc}
\widetilde{U}_{(t,b)} & \supseteq & \widetilde{U}_{(t,a)}\\
\cup| & & \cup|\\
\widetilde{U}_{(s,b)} & \supseteq & \widetilde{U}_{(s,a)}
\end{array}. \tag{23}$$

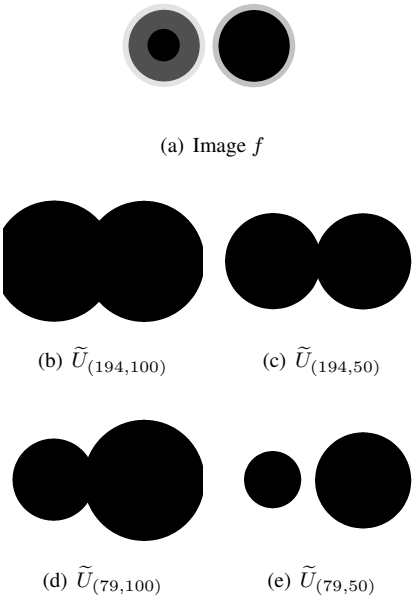

(a) Image f

(b) $\widetilde{U}_{(194,100)}$ (c) $\widetilde{U}_{(194,50)}$

(d) $\widetilde{U}_{(79,100)}$ (e) $\widetilde{U}_{(79,50)}$

Figure 4. A toy example of the distance transform bi-filtration (18) of images of the size 800×600 pixels. In this bi-filtration, we consider the sets of black pixels. The darker the image, the larger the set. The based image f is defined as in Figure 1.

Proof. Because $s \leq t$, $f_t \leq f_s$. By Proposition 2, $\mathrm{supp}(f_t) \subseteq \mathrm{supp}(f_s)$. Therefore, $T_d(f_s) \leq T_d(f_t)$ and $\widetilde{T}_d(f_t) \leq \widetilde{T}_d(f_s)$ by Proposition 4. Hence $\mathcal{T}_d(f_s) \leq \mathcal{T}_d(f_t)$. The row relations in (20), (21), and (22) follow from Proposition 2. □

Example 2. *Consider grayscale image*

$$f = \begin{matrix} 3 & 2 & 2 \\ 2 & 0 & 0 \\ 2 & 0 & 0 \end{matrix} \quad \textit{with } P = \begin{matrix} \bullet & \bullet & \bullet \\ \bullet & \bullet & \bullet \\ \bullet & \bullet & \bullet \end{matrix}. \tag{24}$$

Let d_2 be the 2-norm distance function on P. For $s = 1$ and $t = 2$, we have

$$f_t = \begin{matrix} 1 & 0 & 0 \\ 0 & 0 & 0 \\ 0 & 0 & 0 \end{matrix} \quad \textit{and} \quad f_s = \begin{matrix} 1 & 1 & 1 \\ 1 & 0 & 0 \\ 1 & 0 & 0 \end{matrix}. \tag{25}$$

Hence

$$\begin{aligned} T_{d_2}(f_t) &= \begin{matrix} 0 & 1 & 2 \\ 1 & \sqrt{2} & \sqrt{5} \\ 2 & \sqrt{5} & \sqrt{8} \end{matrix}, \; T_{d_2}(f_s) = \begin{matrix} 0 & 0 & 0 \\ 0 & 1 & 1 \\ 0 & 1 & 2 \end{matrix}, \\ \widetilde{T}_{d_2}(f_t) &= \begin{matrix} 1 & 0 & 0 \\ 0 & 0 & 0 \\ 0 & 0 & 0 \end{matrix}, \; \widetilde{T}_{d_2}(f_s) = \begin{matrix} \sqrt{2} & 1 & 1 \\ 1 & 0 & 0 \\ 1 & 0 & 0 \end{matrix}. \end{aligned} \tag{26}$$

For $a = 0.5$ and $b = 1.4$,

$$\begin{aligned} T_{d_2}(f_t)_b &= \begin{matrix} 0 & 0 & 1 \\ 0 & 1 & 1 \\ 1 & 1 & 1 \end{matrix}, \; T_{d_2}(f_t)_a = \begin{matrix} 0 & 1 & 1 \\ 1 & 1 & 1 \\ 1 & 1 & 1 \end{matrix}, \\ T_{d_2}(f_s)_b &= \begin{matrix} 0 & 0 & 0 \\ 0 & 0 & 0 \\ 0 & 0 & 1 \end{matrix}, \; T_{d_2}(f_s)_a = \begin{matrix} 0 & 0 & 0 \\ 0 & 1 & 1 \\ 0 & 1 & 1 \end{matrix}. \end{aligned} \tag{27}$$

Similarly, for the anti-distance transform:

$$\begin{aligned} \widetilde{T}_{d_2}(f_t)_b &= \begin{matrix} 0 & 0 & 0 \\ 0 & 0 & 0 \\ 0 & 0 & 0 \end{matrix}, \; \widetilde{T}_{d_2}(f_t)_a = \begin{matrix} 1 & 0 & 0 \\ 0 & 0 & 0 \\ 0 & 0 & 0 \end{matrix}, \\ \widetilde{T}_{d_2}(f_s)_b &= \begin{matrix} 1 & 0 & 0 \\ 0 & 0 & 0 \\ 0 & 0 & 0 \end{matrix}, \; \widetilde{T}_{d_2}(f_s)_a = \begin{matrix} 1 & 1 & 1 \\ 1 & 0 & 0 \\ 1 & 0 & 0 \end{matrix}. \end{aligned} \tag{28}$$

This induces the bi-filtration (23)*.*

Note that the nets of preimages of zero induced by (20) and (22) are not bi-filtration since the index orders between index set $\mathbb{Z}^2$ and sets of pixels are not consistent. However, by re-defining the partial orders on $\mathbb{Z}^2$, one may obtain different bi-filtrations. For example, if we define $U_{(\alpha,\beta)} = \mathrm{supp}(T_d(f_\alpha)_\beta) = \mathbb{Z}^2 \setminus (T_d(f_\alpha)_\beta)^{-1}(0)$ and $(x_1, y_1) \leq' (x_2, y_2)$ if and only if $x_1 \leq x_2$ and $y_1 \geq y_2$, then for $s \leq t$ and $a \leq b$,

$$\begin{array}{ccc} U_{(t,b)} & \subseteq & U_{(t,a)} \\ \cup\mathrm{l} & & \cup\mathrm{l} \\ U_{(s,b)} & \subseteq & U_{(s,a)} \end{array} \tag{29}$$

is a bi-filtration for the new partial order $\leq'$ on $\mathbb{Z}^2$. In other words, the index order on $\mathbb{Z}^2$ could be freely modified for different tasks. By choosing suitable indexes, homology of bi-filtrations induced by equations (20), (21), and (22) provide concrete examples of multi-persistence. As we showed in Example 1, except the topological barcodes from thresholding, the persistent homology on the bi-filtration may reveal additional geometric information for images.

4. Application to Firn

Understanding the number and average size of pores within a firn layer is important for modeling air flow through the firn column. As firn layers are buried, they undergo densification with depth due to the overburden pressure of the accumulating snow at the surface. This causes the number of pores, as well as the volume of those pores, to shrink with depth. Ultimately, the firn layers reach the density of glacial ice at the bottom of the firn column, and the interconnected pore space is transformed into individual closed-off bubbles. These bubbles trap a direct sample of atmospheric air, and make up an important paleoclimate record of past

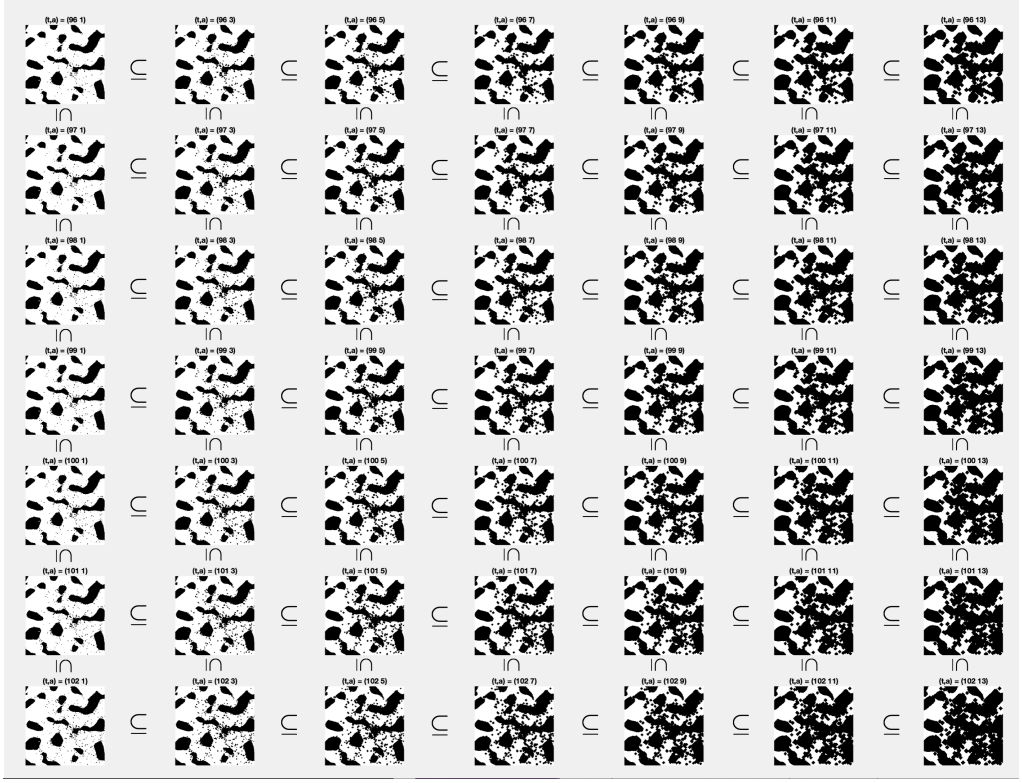

Figure 5. Illustration of the distance transform bi-filtration (18). In this bi-filtration, we consider the sets of black pixels. The darker the image, the larger the set.

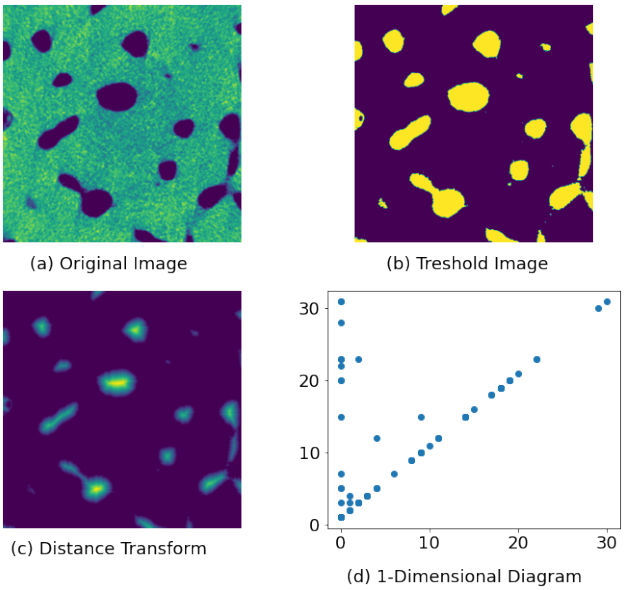

Figure 6. The workflow for extracting a distance transform persistence diagram

atmospheric composition within the glacial ice. A better understanding of the size and number of pores with depth in the firn will help to improve the age estimates of the trapped atmospheric samples within those bubbles.

4.1. Description of the dataset

The firn dataset used in this study comes from a firn core drilled at the NEEM Drilling Camp, Greenland in 2009. From the main core, 1x1x1.5 cm samples were cut at selected depths and scanned with the micro-CT. Reconstructions of the micro-CT data resulted in a stack of approximately 900 cross-sectional images representing the volume of the sample. Each cross-sectional image is approximately 500x500 pixels with a pixel resolution of 15 µm. Here we analyze the samples from 7, 23, 47, 59, and 78 m depth, which span the full range of depths in the NEEM firn column.

4.2. Results

The firn images are grayscale images whose pixel values are integers between 0 and 255. Given a grayscale image, for each integer $t \in \{0, 1, \ldots 255\}$, we can threshold the image to extract a binary image. On each of these threshold images, we apply the distance transform. Next, we compute persistent homology on these images, and extract the relevant statistics from the resulting diagrams. Figure 6 illustrates the common practice, where (a) is a firn image, (b) is a thresholded binary image, (c) the distance transform of

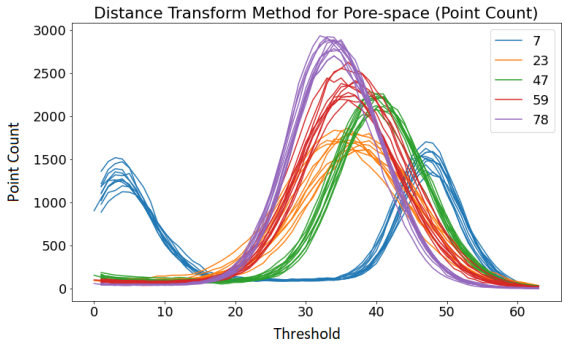

Figure 7. This displays n_t vectors for five depths of firn-core samples. $t = 4i$ for $i = 1, 2, 3, \cdots, 64$. For each depth, 10 images were sampled.

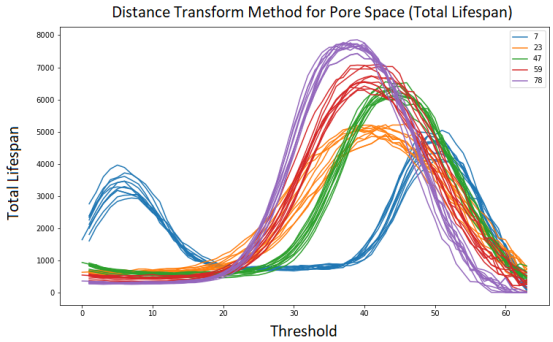

Figure 8. This displays L_t vectors for five depths of firn-core samples. $t = 4i$ for $i = 1, 2, 3, \cdots, 64$. For each depth, 10 images were sampled.

the (b), and (d) is the persistence diagram of (c).

In this work, we consider the bi-filtration $\{\widetilde{U}_{(t,a)}\}$ in (18). Figure 5 shows an example of this bi-filtration. For each t, we consider the persistence diagram along the vertical path, i.e. $D(\{\widetilde{U}_{(t,a)}\}_{a=1}^{M})$. For each persistence diagram along the vertical path, we use the number of points in the diagram and the total lifespan, $\sum_{(b,d)\in D} d - b$, i.e.

$$n_t = \#D(\{\widetilde{U}_{(t,a)}\}_{a=1}^{M}); \tag{30}$$

$$L_t = \sum_{(b,d)\in D(\{\widetilde{U}_{(t,a)}\}_{a=1}^{M})} d - b. \tag{31}$$

We consider $t_i = 4i$ for $i = 1, 2, 3, \cdots, 64$. Hence, for each image, both n_t and L_t are of 64-dimensional vector. Both of n_t and L_t reveal something about the underlying image. The n_t vector reveals how many generators there were and can help us count the number of contiguous ice or air regions. The L_t vector gives us an idea of how big these contiguous regions are. Figure 7 shows a plot of the n_t vector for 10 sample images of five different depths of ice-core samples. We note the image shows a nice separation of these values by depth. Similarly, Figure 8 shows a plot of the L_t vector for the same 10 sample images of five different depths of ice-core samples. We note the image shows a nice separation of these values by depth. We also note that it takes about 120 seconds to process one slice and produce a vector. In the demonstrations and experiments, the persistence diagrams were computed by the software `GUDHI` [31]. The distance transforms were computed with OpenCV [1].

4.3. Discussion

From Figure 7, we observe that the shapes of the point-count curves vary with respect to depth. At each depth, the ten curves from the ten randomly selected images in the sample stack are very similar, yet not the same. The differences between the ten curves for each sample are due to heterogeneity within the firn samples themselves. The curves suggest that images at one sample depth have similar characteristics, and that samples from different depths are distinct.

Additionally, The group of point-count curves for samples 23, 47, 59, and 78m are unimodal while the curves for sample 7m is bimodal. At very shallow depths in the firn column, such as in sample 7m, the amount of ice- and pore-space is relatively equal within the sample. On the other hand, the ice-space dominates the firn microstructure for the samples at greater depths because of their much larger densities. Therefore, as we scan through the threshold values for shallow firn samples, we can expect a bimodal distribution of the point count. The transition between bimodal and unimodal point-count curves likely corresponds to a consequential shift in firn density.

In Figure 8, we observe the maximum values of the curves, which reveal the size and complexity of the ice space for each firn sample. In general, as images become darker and darker, as the threshold value increases, more white holes will be formed. If these images contain a large portion of white pixels, it will take a lot of effort to fill in all the white regions, and therefore, the total lifespan would be larger. Looking at the firn samples, the maximum count values are approximately 4000 for 7m (blue curves), 5000 for 23m (orange curves), 6000 for 47m (green curves), 6500 for 59m (red curves), and 8000 for 78m (purple curves). As we go deeper in the firn column, the firn layers contain more ice space and have increasingly simple structures. Therefore, we expect the deeper samples to have larger point counts than shallower samples, as we've seen here, because the complexity decreases with depth and the portion of white space (ice space) increases with depth.

References

[1] G. Bradski. The OpenCV Library. *Dr. Dobb's Journal of Software Tools*, 2000.

[2] C. D. Cantrell. *Modern Mathematical Methods for Physicists and Engineers*. Cambridge University Press, 2000.

[3] Gunnar Carlsson. Topology and data. *Bulletin of the American Mathematical Society*, 46(2):255–308, 2009.

[4] Gunnar Carlsson, Gurjeet Singh, and Afra J Zomorodian. Computing multidimensional persistence. *Journal of Computational Geometry*, 1(1):72–100, 2010.

[5] Frédéric Chazal and Bertrand Michel. An introduction to topological data analysis: fundamental and practical aspects for data scientists. *arXiv preprint arXiv:1710.04019*, 2017.

[6] Herbert Edelsbrunner and John Harer. *Computational topology: an introduction*. American Mathematical Soc., 2010.

[7] Herbert Edelsbrunner, David Letscher, and Afra Zomorodian. Topological persistence and simplification. In *Proceedings 41st Annual Symposium on Foundations of Computer Science*, pages 454–463. IEEE, 2000.

[8] Adélie Garin and Guillaume Tauzin. A topological" reading" lesson: Classification of mnist using tda. In *2019 18th IEEE International Conference On Machine Learning And Applications (ICMLA)*, pages 1551–1556. IEEE, 2019.

[9] Robert Ghrist. Barcodes: the persistent topology of data. *Bulletin of the American Mathematical Society*, 45(1):61–75, 2008.

[10] Marvin J. Greenberg and John R.Harper. *Algebraic Topology, A First Course*. Addison-Wesley Publishing Company, 1980.

[11] Heather A Harrington, Nina Otter, Hal Schenck, and Ulrike Tillmann. Stratifying multiparameter persistent homology. *SIAM Journal on Applied Algebra and Geometry*, 3(3):439–471, 2019.

[12] Allen Hatcher. *Algebraic topology*. Cambridge Univ. Press, Cambridge, 2000.

[13] AL Herring, Vanessa Robins, and AP Sheppard. Topological persistence for relating microstructure and capillary fluid trapping in sandstones. *Water Resources Research*, 55(1):555–573, 2019.

[14] Chuan-Shen Hu and Yu-Min Chung. On the conditions of absorption property for morphological opening and closing. *ArXiv*, 2020.

[15] Fei Jiang, Takeshi Tsuji, and Tomoyuki Shirai. Pore geometry characterization by persistent homology theory. *Water Resources Research*, 54(6):4150–4163, 2018.

[16] T. Kaczynski, K. Mischaikow, and M. Mrozek. *Computational Homology*. Applied Mathematical Sciences. Springer New York, 2004.

[17] MA Kader, AD Brown, PJ Hazell, V Robins, JP Escobedo, and M Saadatfar. Geometrical and topological evolution of a closed-cell aluminium foam subject to drop-weight impact: An x-ray tomography study. *International Journal of Impact Engineering*, 139:103510, 2020.

[18] E.F. Krause. *Taxicab Geometry: An Adventure in Non-Euclidean Geometry*. Dover Books on Mathematics. Dover Publications, 2012.

[19] Michael Lesnick. The theory of the interleaving distance on multidimensional persistence modules. *Foundations of Computational Mathematics*, 15(3):613–650, 2015.

[20] Michael Lesnick and Matthew Wright. Computing minimal presentations and bigraded betti numbers of 2-parameter persistent homology. *arXiv preprint arXiv:1902.05708*, 2019.

[21] Chul Moon, Scott A Mitchell, Jason E Heath, and Matthew Andrew. Statistical inference over persistent homology predicts fluid flow in porous media. *Water Resources Research*, 55(11):9592–9603, 2019.

[22] Laurent Najman and Hugues Talbot. *Mathematical Morphology*. Wiley-ISTE, 1d edition, 2010.

[23] Ippei Obayashi, Yasuaki Hiraoka, and Masao Kimura. Persistence diagrams with linear machine learning models. *Journal of Applied and Computational Topology*, 1(3):421–449, 2018.

[24] John Tinsley Oden and Leszek Demkowicz. *Applied Functional Analysis*. Textbooks in Mathematics. CRC Press, 2017.

[25] Alice Patania, Francesco Vaccarino, and Giovanni Petri. Topological analysis of data. *EPJ Data Science*, 6:1–6, 2017.

[26] Vanessa Robins, Mohammad Saadatfar, Olaf Delgado-Friedrichs, and Adrian P Sheppard. Percolating length scales from topological persistence analysis of micro-ct images of porous materials. *Water Resources Research*, 52(1):315–329, 2016.

[27] Martina Scolamiero, Wojciech Chachólski, Anders Lundman, Ryan Ramanujam, and Sebastian Öberg. Multidimensional persistence and noise. *Foundations of Computational Mathematics*, 17(6):1367–1406, 2017.

[28] Jean Serra. *Image Analysis and Mathematical Morphology*. Number 1 in Image Analysis and Mathematical Morphology. Academic Press, 1984.

[29] Pierre Soille. *Morphological Image Analysis: Principles and Applications*. Springer-Verlag New York, Inc., Secaucus, NJ, USA, 2 edition, 2003.

[30] Mohmad Mohsin Thakur, Felix Kim, Dayakar Penumadu, and Anna Herring. Pore space and fluid phase characterization in round and angular partially saturated sands using radiation-based tomography and persistent homology. *Transport in Porous Media*, 137(1):131–155, 2021.

[31] The GUDHI Project. *GUDHI User and Reference Manual*. GUDHI Editorial Board, 3.4.1 edition, 2021.

[32] James W. Vick. *Homology Theory, A Introduction to Algebraic Topology*. Springer-Verlag Publishing Company, Second Edition, 1973.

[33] Larry Wasserman. Topological data analysis. *Annual Review of Statistics and Its Application*, 5:501–532, 2018.

[34] Q. Ye. The signed euclidean distance transform and its applications. In *9th International Conference on Pattern Recognition*, pages 495,496,497,498,499, Los Alamitos, CA, USA, nov 1988. IEEE Computer Society.

[35] Afra Zomorodian. Topological data analysis. *Advances in applied and computational topology*, 70:1–39, 2012.